Visible-light Ag/AgBr/ferrihydrite catalyst with enhanced heterogeneous photo-Fenton reactivity via electron transfer from Ag/AgBr to ferrihydrite

Yanping Zhu[a,b,c], Runliang Zhu[a,*], Lixia Yan[a,b], Haoyang Fu[a,b], Yunfei Xi[c,*], Huijun Zhou[a,b], Gangqiang Zhu[d], Jianxi Zhu[a], Hongping He[a]

[a] CAS Key Laboratory of Mineralogy and Metallogeny, Guangdong Provincial Key Laboratory of Mineral Physics and Materials, Guangzhou Institute of Geochemistry, Chinese Academy of Sciences(CAS), Guangzhou, 510640, China
[b] University of Chinese Academy of Sciences, Beijing, 100049, China
[c] School of Earth, Environmental and Biological Sciences, Queensland University of Technology (QUT), Brisbane, Queensland, 4001, Australia
[d] School of physics and information technology, Shaanxi Normal University, Xi'an, 710062, PR China
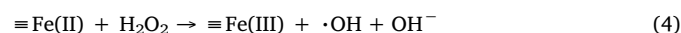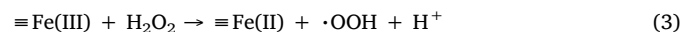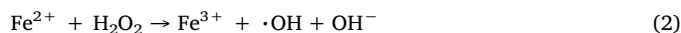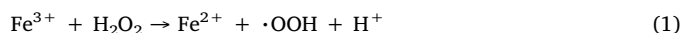
ARTICLE INFO

ABSTRACT

Herein, we have reported an effective strategy to solve the rate-limiting step in a heterogeneous Fenton reaction, i.e., the generation of Fe(II) from Fe(III), which also inevitably consumes a large amount of H_2O_2. For the first time, a novel heterogeneous photo-Fenton catalyst - Ag/AgBr/ferrihydrite (Ag/AgBr/Fh) was successfully developed by combing AgBr with ferrihydrite (Fh) and then in-situ generating Ag nanoparticles on the surface of AgBr/Fh. This strategy can introduce photo-generated electrons from semiconductor-based plasmonic photocatalysts to heterogeneous Fenton catalysts and significantly increase the efficiency to degrade contaminants. The presence of both AgBr and Ag nanoparticles was proved by a combination of structural characterization studies (i.e., XRD, SEM, TEM, and XPS). Under visible light irradiation, the generated Fe(II) on the samples and the degradation rate constants of bisphenol A (BPA) followed the same order: Ag/AgBr/Fh > AgBr/Fh > Fh, which could be attributed to the accelerated reduction of Fe(III) to Fe(II) by the photo-generated electrons from AgBr and Ag nanoparticles, and also profit from the strong electron trapping ability of Ag nanoparticles in separating the electron-hole pairs of AgBr. The Ag/AgBr/Fh system could produce more hydroxyl radicals (•OH), and its catalytic performance was less affected by decreasing H_2O_2 concentration, which suggested a more efficient utilization of H_2O_2. The Ag/AgBr/Fh system exhibits relatively high photo-Fenton reactivity even at neutral pH. In addition, a much lower Fe^{3+} dissolution indicates that a large portion of the contribution is from the direct heterogeneous Fenton reaction in this system.

1. Introduction

As one of the most studied advanced oxidation processes (AOPs), heterogeneous Fenton system can remove stubborn contaminants under acidic or even neutral pH conditions without producing a large amount of ferric − hydroxide sludge, and it has been regarded as a promising alternative to the homogeneous Fenton reaction [1–8]. There are two main reaction routes between solid iron-based catalysts and H_2O_2: (i) the reaction of the leached Fe from catalysts with H_2O_2 (i.e., a homogeneous Fenton reaction) (Eqs. (1) and (2)), and (ii) the reaction of surface Fe ($\equiv$Fe(III)) with H_2O_2 (Eqs. (3) and (4)) [2,9]. Both routes can generate highly reactive hydroxyl radicals (·OH) to degrade most organic contaminants to the mineral end-products in a non-selective way.

$$Fe^{3+} + H_2O_2 \rightarrow Fe^{2+} + \cdot OOH + H^+ \tag{1}$$

$$Fe^{2+} + H_2O_2 \rightarrow Fe^{3+} + \cdot OH + OH^- \tag{2}$$

$$\equiv Fe(III) + H_2O_2 \rightarrow \equiv Fe(II) + \cdot OOH + H^+ \tag{3}$$

$$\equiv Fe(II) + H_2O_2 \rightarrow \equiv Fe(III) + \cdot OH + OH^- \tag{4}$$

Nevertheless, the slow generation rate of Fe^{2+}/Fe(II) and the consumption of a large amount of H_2O_2 in these two processes (Eqs. (1) and (3)) are the two inherent drawbacks in the heterogeneous Fenton reaction, which inevitably weaken the reaction performance, raise the costs of the process, and hinder the large-scale applications of this technique in water treatment [2,9,10]. Many studies, therefore, tried to introduce adscititious electrons to accelerate the generation rate of Fe^{2+}/Fe(II) [9,11–21]. For example, some carboxylic acids (e.g.,

oxalate and citrate) [11,12], carbon materials (e.g., graphene oxide, carbon nanotubes and polyhydroxy fullerene) [13–15], and sulfide irons of metal sulfides (e.g., FeS_2, ZnS and MoS_2) [16–18] can directly transfer their electrons to heterogeneous catalysts and result in an efficient generation of Fe^{2+}/Fe(II). Recently, the studies from our group, together with several other publications, showed that, under light irradiation, semiconductors (e.g., $BiVO_4$, TiO_2, and g-C_3N_4) could continuously transfer their photo-generated electrons to heterogeneous catalysts [9,19,12–21]; thus evidently accelerate the process and significantly enhance the Fenton reaction activity. Xu et al. [9] further showed that, through a similar strategy, the $BiVO_4$/ferrihydrite complex remained a quite high photo-Fenton reactivity in the degradation of acid red 18 even at neutral pH. Despite these interesting findings and progress, alternative and more effective methods are still of high necessity. In addition, the underlying mechanisms and inherent merits for directly introducing photon-generated electrons to heterogeneous Fenton catalysts in the Fenton reaction processes still need to be further explored. For example, it is necessary to study whether the direct solid phase reduction of Fe(III) by electrons can reduce the dissolution of Fe^{3+} from catalysts and then broader the optimal pH range at the same time.

As is known, Ag/AgBr composite can generate electrons quite efficiently under the irradiation of visible light due to the following reasons: i) AgBr, with a band gap of 2.6 eV, has been proved to be an excellent visible-light-driven photocatalyst [22–25]; ii) Ag nanoparticles deposited on the surface of AgBr can efficiently absorb visible light to generate electrons due to the surface plasmon resonance (SPR) effect [26–30]; iii) the electrons from the conduction band of AgBr can be transferred to Ag nanoparticles due to the Schottky barrier at the Ag–AgBr interface [27,29,31,32]. From the perspective of the excellent properties of Ag/AgBr, we expected that Ag/AgBr should be more effective than conventional semiconductor-based photocatalysts in generating electrons for the reduction of Fe^{3+}/Fe(III) on a heterogeneous Fenton catalyst, thus promote the decomposition of H_2O_2 to ·OH (Eqs. (2) and (4)). Moreover, we hypothesize that once Fe^{3+}/Fe(III) was directly reduced to Fe^{2+}/Fe(II) by photo-generated electrons, the consumption of H_2O_2 for the generation of Fe^{2+}/Fe(II) (Eqs. (1) and (3)) could be minimized, which may evidently reduce the costs of this technique.

Among various heterogeneous Fenton catalysts, ferrihydrite (Fh), as a typical iron (oxyhydr)oxide nano mineral, has attracted many interests recently due to its large specific surface area (SSA > 200 m^2/g), nano-sized structure, and abundant surface Fe−OH groups [9,12,33]. In a Fenton system, the nanostructured properties of Fh can not only increase the contact between Fh, H_2O_2, and contaminants [12,34] but also enable Fh as a good support to disperse functional materials uniformly [9,15,35]. In addition, Matta et al. [16] found that Fh exhibited higher Fenton-like oxidation of 2,4,6-trinitrotoluene than other iron minerals (e.g., lepidocrocite, hematite, and goethite).

With above considerations, for the first time, we have successfully synthesized novel heterogeneous photo-Fenton catalysts (Ag/AgBr/Fh) by loading different amounts of Ag/AgBr on the surface of Fh via a precipitation-photo reduction method. BPA degradation test results have demonstrated that the photo-generated electrons from Ag/AgBr can not only accelerate the generation of Fe^{2+}/Fe(II) but also improve the utilization efficiency of H_2O_2, leading to enhanced photo-Fenton reactivity. On the other hand, direct solid phase reduction of Fe(III) by these electrons can enhance the structural stability of the catalysts and broaden the optimal pH range. Related reaction mechanisms, such as the release of Fe^{3+} in solution, the concentration of Fe(II) on catalysts, the effect of decreased H_2O_2 concentration, and the concentration of ·OH were thoroughly studied.

2. Experiment

2.1. Materials

Fe $(NO_3)_3$·$9H_2O$ (AR), $AgNO_3$ (AR), NaBr (AR), NaOH (AR), HCl (AR), and hydrogen peroxide (30 wt. %) were purchased from Shanghai Chemical Reagent Corporation, China. Benzoic acid (99.5%) and p-hydroxybenzoic acid (99%) were obtained from Aladdin Industrial Corporation (Shanghai, China). Bisphenol A and $K_2TiO(C_2O_4)_2$ was purchased from Macklin Reagent Company. All reagents were used as received.

2.2. Synthesis of Fh

Two-line Fh was synthesized according to the following process: Fe $(NO_3)_3$·$9H_2O$ (1 M, 40 mL) and NaOH (6 M, 20 mL) were slowly and simultaneously titrated into a beaker under vigorous stirring for 3 h and the pH value was controlled at 7 ± 0.1 [9]. Then, the mixture was centrifuged and washed several times using ultra-pure water and ethanol. After being freeze-dried, the sample was ground to pass through a 200-mesh sieve.

2.3. Synthesis of AgBr/Fh and Ag/AgBr/Fh

To prepare AgBr/Fh, an appropriate amount of $AgNO_3$ (0.064, 0.128, or 0.192 g) and Fh powder (1 g) were added into 20 mL ultra-pure water. The mixture was sonicated for 30 min and stirred for 60 min to disperse Ag^+ on the surface of Fh thoroughly. After that, 20 mL excess NaBr solution (3.87, 7.74, or 11.63 mM) was added dropwise into the mixture solution to precipitate Ag^+ into AgBr completely. The precipitates were centrifuged and washed thoroughly with ultra-pure water. After being freeze-dried, the materials were ground to pass through a 200-mesh sieve. According to the calculated weight ratio of AgBr to Fh, the resulting materials were labeled as 4%AgBr/Fh, 8%AgBr/Fh, and 12%AgBr/Fh.

To prepare Ag/AgBr/Fh, 1 g 8%AgBr/Fh sample was added to 40 mL ultra-pure water. After stirring for 60 min, 10 mL methanol (as a hole scavenger) was added to the above suspension. Subsequently, the resulting suspension was placed under irradiation of a 300 W mercury lamp (BL-GHX-V, Shanghai Depai Biotech. Co. Ltd., China) for 30 min. The obtained precipitate was washed with ultra-pure water and alcohol several times, and then freeze-dried. The sample was labeled as 8%Ag/AgBr/Fh.

2.4. Characterization

XRD patterns were obtained using a Bruker D8 ADVANCE X-ray diffractometer (Karlsruhe, Germany). The measurements were operated at 40 kV and 40 mA with Cu Kα radiation, and all samples were scanned from 3° to 80° with a scanning speed of 3°/min. The scanning electron microscopy (SEM) images were recorded by a field emission scanning electron microscopy (Carl Zeiss SUPRA55SAPPHIR). Transmission electron microscopy (TEM) images were obtained using FEI Talos F200S instrument at an acceleration voltage of 200 kV with energy dispersive X-ray spectroscopy (EDS) (Super X) for the determination of metal composition. X-ray photoelectron spectroscopy (XPS) analyses were carried out by a Thermo Fisher Scientific K-Alpha spectrometer. The C1s peak from the adventitious carbon-based contaminant with bind energy of 284.80 eV was used as the reference for calibration. The UV–vis diffuse reflectance spectra (DRS) were recorded on a UV–vis spectrometer (Shimadzu UV-2550) using $BaSO_4$ as an absorbance standard. The AgBr photoanode was used as the working electrode; a Pt sheet served as the counter electrode. Ag/AgCl (saturated KBr) electrode was used as the reference electrode at room temperature.

2.5. Photo-Fenton catalytic experiments

The photo-Fenton degradation of BPA by the as-prepared materials was monitored in a photochemical reaction instrument (PCX50 A Discover, Beijing Perfectlight Technology Co., Ltd, Beijing, China). A 5 W LED lamp (148.5 mW/cm^2) was used as a cold light source. Details of the photo-Fenton reaction setup and LED lamps were provided (Figs. S1 and S2, and Table S1). The initial pH value of the solution (pH = 3) was adjusted by adding 0.1 mol/L NaOH and HNO$_3$. Before irradiation, a mixture of 50 mg catalyst and 50 mL BPA (30 mg/L) solution was vigorously stirred in the dark for 30 min to reach the adsorption-desorption equilibrium. After that, 0.5 mL 1 M H$_2$O$_2$ was dropped into the above solution. At given time intervals, certain volume of the suspension was collected and filtered immediately with 0.22 μm membrane filters.

The concentration of the filtrates was quantitatively analyzed using an Agilent 1260 HPLC equipped with a Luna 5μ C18 column (250 mm) and a UV absorbance detector according to the method of Samanidou et al. 2014 with some modifications [36]. A mobile phase of acetonitrile and water (50:50, v/v) at a flow rate of 0.8 mL/min and an injection volume of 20 μL were used for this experiment, and the analysis wavelength was selected as 230 nm. The detection limit of BPA in this study was about 0.01 mg/L. The total organic carbon (TOC) was measured by using a Shimadzu TOC-V total organic carbon analyzer. The concentration of H$_2$O$_2$ was calculated by adding 3 mL of K$_2$TiO(C$_2$O$_4$)$_2$ (10 mM in 2.4 M H$_2$SO$_4$) to form an orange complex (pertitanic acid) with maximum absorption at 400 nm [9,37]. The concentration of pertitanic acid was measured via UV–vis spectroscopy (759S, Shanghai JingHua Instrument Co. Ltd., China).

The concentration of Fe(II) on as-prepared samples were measured according to the method of Xu et al. [9] with some modifications, which is also a common method for the measurement of Fe(II) in the iron ore [38]. At a given time interval, the suspension was centrifuged, and the supernatant liquid was removed immediately. 1 mL 6 M hydrochloric acid, 0.2 g Na$_2$CO$_3$, and 2 mL 10 M NH$_4$F were added to dissolve Fh totally and prevent Fe(II) from being oxidized to Fe(III). After that, 1 mL CH$_3$COONH$_4$ − CH$_3$COOH buffer solution (pH 4.2) and 1 mL 0.5% (m/v) o-phenanthroline were added into above solution to form an orange complex in acidic solution. The concentration of complex was measured via UV–vis spectroscopy with maximum absorption at 510 nm.

In this study, the oxidation of benzoic acid (BA at 10 mM) to p-hydroxybenzoic acid (p-HBA) at an initial pH value of 3 was used as a probe reaction for quantifying the production of ·OH in the process of photo-Fenton catalysis [39]. The p-HBA was also quantitatively analyzed using the Agilent 1260 HPLC equipped with a Luna 5μ C18 column (250 mm). The mobile phase was a mixture of 0.1% trifluoroacetic acid aqueous solution and acetonitrile (65:35, v/v) at a flow rate of 1 mL/min, with the detection wavelength at 255 nm [39,40].

3. Results and discussion

3.1. Structural characterization results

The XRD patterns of Fh, AgBr/Fh, and 8%Ag/AgBr/Fh are presented in Fig. 1.

For Fh, there are two broad reflections at 35° and 63°, well consistent with the previous report for 2-line Fh [9,10]. After introducing AgBr, six distinct reflections at 26.7°, 31.0°, 44.3°, 55.0°, 64.5°, and 73.3° are observed, which can be indexed to the (111), (200), (220), (222), (400), and (420) diffraction planes of AgBr, respectively (JCPDS 06-0438). For 8%Ag/AgBr/Fh, however, no reflections assigned to Ag° can be detected, probably due to its relatively low content and low crystallinity because of the high dispersity of Ag nanoparticles [41].

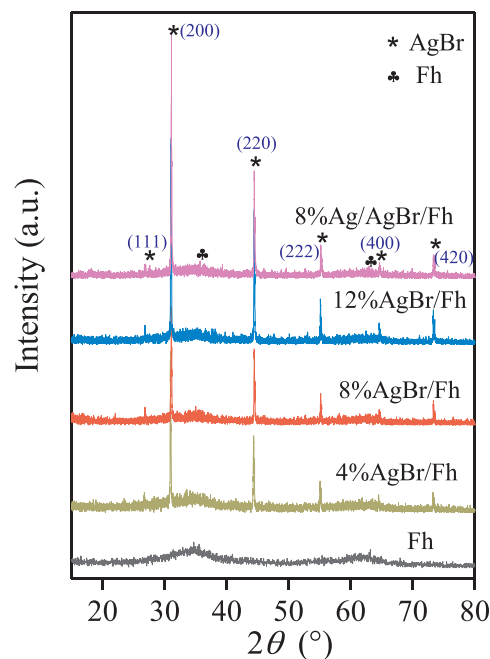The morphologies of Fh, AgBr, Ag/AgBr, 8%AgBr/Fh, and 8%Ag/

Fig. 1. XRD patterns of the as-prepared samples.

AgBr/Fh were examined by SEM (Fig. 2). Fh presents the aggregations of nanoparticles, while AgBr shows the gathering of 1–3 μm particles. As for the Ag/AgBr sample, some Ag nanoparticles are deposited on the surface of AgBr. The SEM image of 8%AgBr/Fh shows uniformly dispersed AgBr particles with a size of 100–500 nm on the surface of Fh, which suggests that Fh should have an obvious tailoring effect on the aggregated AgBr particles. Ag nanoparticles with diameters in the range of 5–50 nm are also observable on the surface of 8%Ag/AgBr/Fh, which were also observed in other Ag/AgBr-based photocatalysts [42,43].

The microstructural and morphological details of 8%Ag/AgBr/Fh were further investigated by TEM and HRTEM (Fig. 3). The Ag/AgBr nanoparticles with the size of 50–200 nm are observed on the surface of Fh. The interplanar spacing of 0.330 nm corresponds to the (111) plane of AgBr, while those at 0.235 and 0.204 nm can be attributed to the (111) and (200) plane of Ag nanoparticles, respectively [44,45]. These results further confirm the existence of AgBr and Ag nanoparticles on 8%Ag/AgBr/Fh.

The XPS measurements were carried out to elucidate the chemical state of the elements on the surface of 8%Ag/AgBr/Fh (Fig. 4). The survey spectrum proves the existence of Fe, O, Ag, and Br elements on the surface of the composite. For the XPS spectrum of Fe 2p, two peaks at 710.35 and 711.72 eV are attributed to the binding energies of Fe (III)–O on Fh [12,46,47]. According to Vempati and Loeppert 1990 [47], the peak at 711.72 eV is attributed to octahedrally-coordinated lattice Fe^{3+}. Due to that Fe in Fh is in a high-spin or paramagnetic state, the other peak at 710.35 eV could be a Fe(III) satellite peak, which results from a multiple splitting of Fe 2p sublevels.

The XPS spectrum of Ag 3d displays two distinct peaks, which can be further divided into four different peaks. In particular, the peaks at 368.5 and 374.5 eV are attributed to Ag°, while those at 367.9 and 373.9 eV correspond to the Ag$^+$ of AgBr [48]. According to a method from Tang et al. 2014 [49], the XPS Ag 3d spectra of as-prepared 8%Ag/AgBr/Fh and 8%AgBr/Fh were normalized and then subtracted from 8%Ag/AgBr/Fh to 8%AgBr/Fh, as shown in Fig. S3a, and the detailed method was also shown in the supplementary material. Two apparent peaks at 368.5 and 374.5 eV are observed, indicating the presence of Ag° in 8%Ag/AgBr/Fh. The Br 3d spectrum consists of two peaks of Br 3d$_{5/2}$ and Br 3d$_{3/2}$, with binding energies of 68.5 and 69.7 eV, respectively [27]. The XPS analysis also confirms the presence
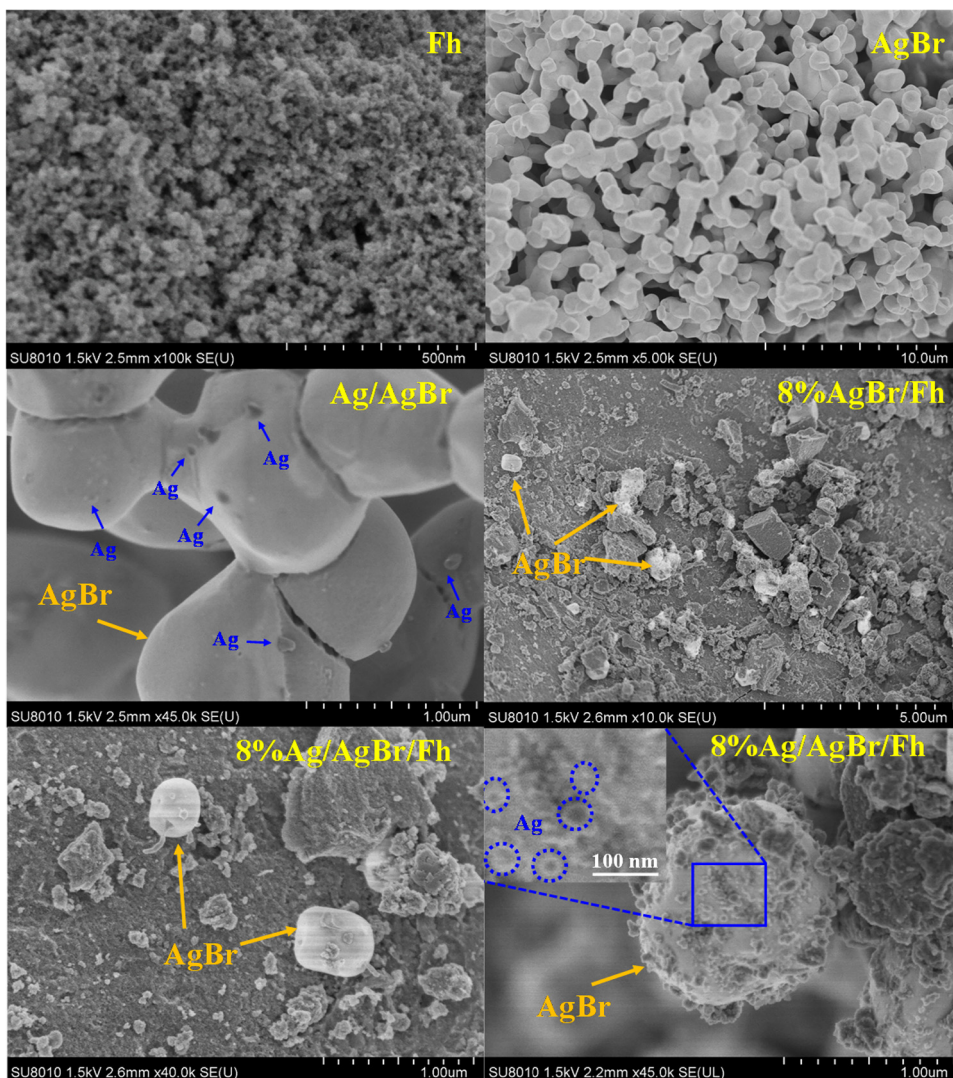
Fig. 2. SEM images of Fh, AgBr, Ag/AgBr, 8%AgBr/Fh, and 8%Ag/AgBr/Fh.

of Ag° on 8%Ag/AgBr/Fh.

The optical absorptions of the as-prepared samples were also measured by UV–vis diffuse reflectance spectroscopy (Fig. 5a). Pure Fh presents broad absorption over the whole region. After introducing AgBr, the DRS intensity of AgBr/Fh increases with increasing AgBr content. Moreover, the DRS intensity of 8%Ag/AgBr/Fh further
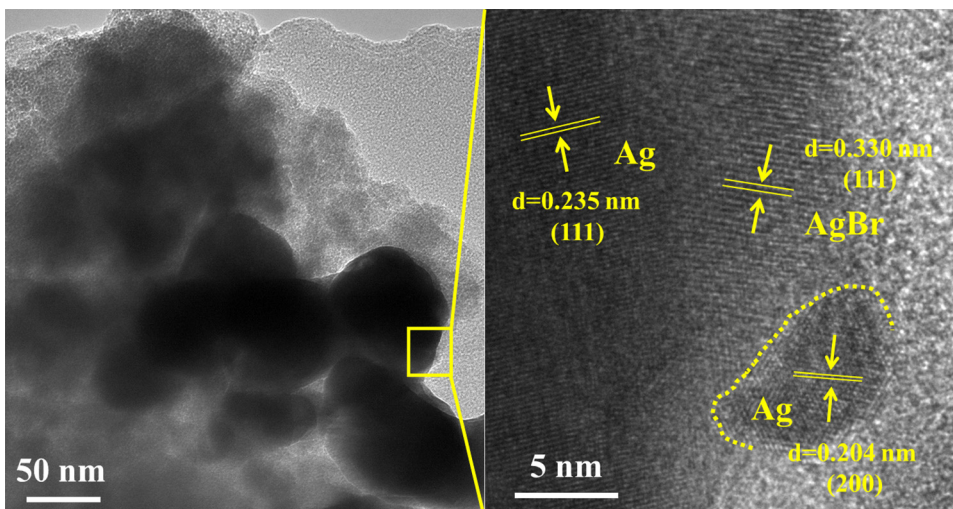

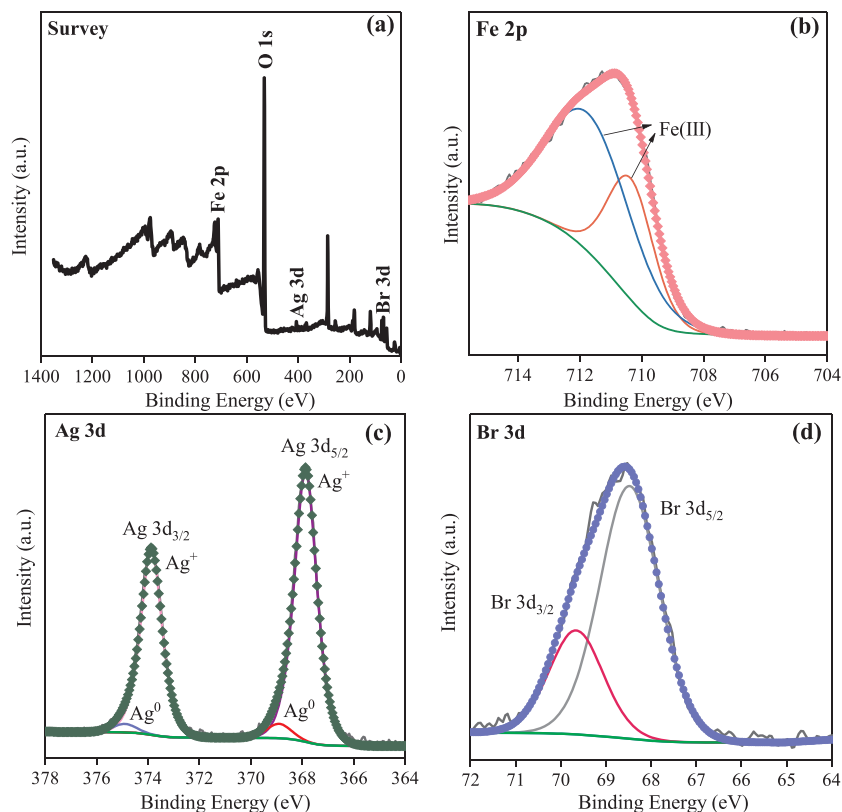**Fig. 3.** TEM and HRTEM images of 8%Ag/AgBr/Fh.

Fig. 4. XPS spectra of 8%Ag/AgBr/Fh sample: (a) Survey, (b) Fe 2p, (c) Ag 3d, and (d) Br 3d.

increases in the region of visible light after Ag nanoparticles being generated on the surface of AgBr. This phenomenon was also observed in other studies involving Ag/AgBr-based photocatalysts [50,51]. Zhang et al. [51] deduced that the increased absorption of visible light might be attributed to the SPR effect of Ag nanoparticles.

The flat band potential (E_{fb}) of pure AgBr was measured by the Mott-Schottky test (Fig. 5b). The positive slope in Mott–Schottky plots indicates that AgBr is an n-type semiconductor. The E_{fb} is estimated to be -0.93 V vs. Ag/AgCl (a reference electrode; ≈0.08 V vs. NHE) by extrapolating the curve to $1/C^2 = 0$. Generally, for n-type semiconductors, the conduction band potential is nearly equal to the flat-band potential. Thus, the conduction band potential of pure AgBr is −1.13 V vs. NHE, well consistent with a previous study [52].
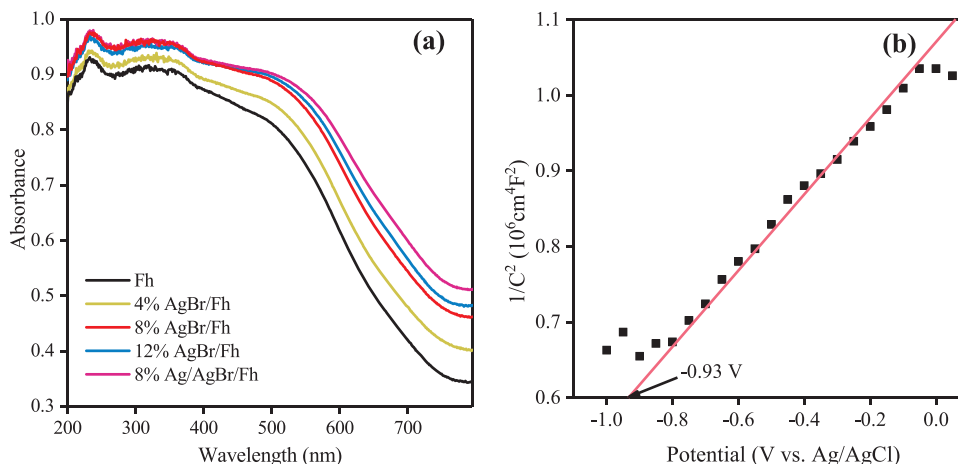
3.2. Photo-Fenton degradation of BPA

Negligible BPA can be degraded in the dark, indicating low adsorption capacity of BPA over these samples (Fig. 6a). After being irradiation by visible light, no apparent degradation can be obtained either by visible light or H_2O_2. About 19% and 51% BPA can be degraded by AgBr and Fh, respectively. After loading AgBr on the surface of Fh, the degradation rate of BPA increases remarkably. The degradation efficiency of BPA on 8%AgBr/Fh can reach 87.7% within 60 min. The degradation kinetics of BPA over these samples were fitted with the pseudo-first-order equation. The apparent rate constants were determined from the regression curves of $-\ln(C/C_0)$ versus irradiation time (Fig. 6b), in which the value of the rate constant (K_{app}) is equal to the corresponding slope of the fitting line. The K_{app} of 8%AgBr/Fh is 0.0259 min^{-1}, which is about 2.6 times as high as that of pure Fh

Fig. 5. (a) UV–vis diffuse reflectance spectra of Ag/AgBr/Fh with various Ag contents; (b) Mott-Schottky plots of AgBr collected at a frequency of 1 kHz.
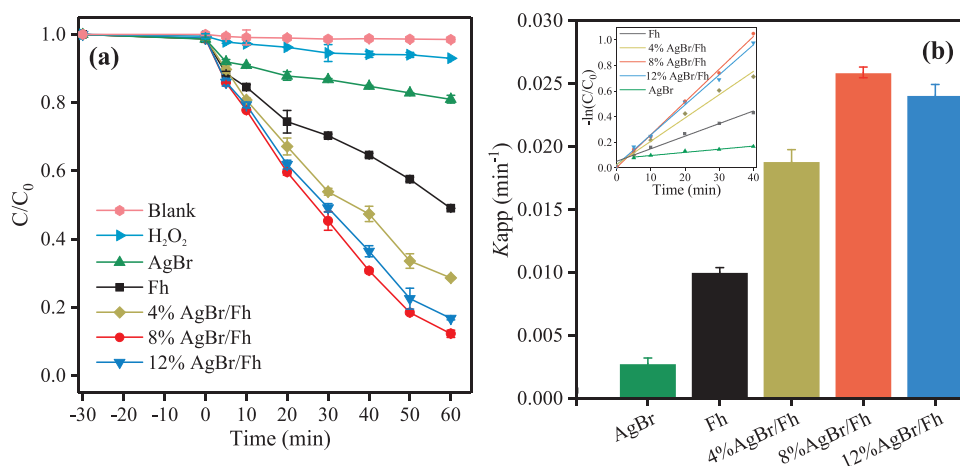
Fig. 6. (a) Degradation kinetics and (b) apparent degradation rate constants of BPA on AgBr/Fh samples under visible light irradiation. Inset of (b): pseudo-first order kinetics for the photocatalytic degradation of BPA on these samples. [Catalyst dosage] = 1 g/L; [BPA] = 30 mg/L; [H_2O_2] = 10 mM; pH = 3.

(0.0101 min^{-1}). This result has further supported previous findings that incorporation semiconductors on the surface of heterogeneous Fenton catalysts can significantly increase their photo-Fenton catalytic activities in the degradation of organic contaminants [53–55]. In addition, the XRD patterns and XPS spectra of AgBr and 8%AgBr/Fh before and after the degradation of BPA were compared (Fig. S4), indicating no Ag° generated in the degradation of BPA by 8%AgBr/Fh.

To further study the photo-Fenton catalytic activity of Ag/AgBr/Fh samples, the experiments for the degradation of BPA by AgBr, Ag/AgBr, 8%AgBr/Fh, and 8%Ag/AgBr/Fh were conducted under visible light irradiation (Fig. 7a). After depositing Ag nanoparticles on the surface, the photo-Fenton catalytic activities of Ag/AgBr and 8%Ag/AgBr/Fh increase evidently, as compared with those of AgBr and 8%AgBr/Fh. The calculated K_{app} in the 8%Ag/AgBr/Fh system is 0.0370 min^{-1}, which is about 3.7 and 1.4 times higher than those in the pure Fh system (0.0101 min^{-1}) and the 8%AgBr/Fh system (0.0259 min^{-1}), respectively (Fig. 7b). These results clearly show that Ag nanoparticles can play an important role in the photo-Fenton reaction.

TOC removal efficiency of BPA was further examined to test the photo-Fenton catalytic activities of the as-prepared samples. The TOC removal in these systems decreases in the order: 8%Ag/AgBr/Fh (68%) > 8%AgBr/Fh (63%) > Fh (50%) (Fig. S5), further indicating the high reactivity of Ag/AgBr/Fh. Above results have proved our hypothesis that combining semiconductors with plasmonic photocatalysts can be an effective strategy to enhance the photo-Fenton reactivity of heterogeneous Fenton catalysts.

The concentrations of Fe^{3+} in the solution of the photo-Fenton

reaction systems were also measured. In the whole reaction process, the concentrations of Fe^{3+} are much lower in the 8%Ag/AgBr/Fh and 8%AgBr/Fh systems than that in the Fh system (Fig. 8a). Specifically, comparing the Fh system with the 8%Ag/AgBr/Fh system, the maximum dissolution of Fe^{3+} decreases from 0.56 to 0.24 mg/L, which suggests that Ag/AgBr can improve the stability of Fh in the photo-Fenton reaction process. Combining with the observed higher photo-Fenton reactivity of 8%Ag/AgBr/Fh and 8%AgBr/Fh than Fh in degradation of BPA (Figs. 6 and 7), we can make the conclusion that direct heterogeneous Fenton reaction (Eq. (3)) should have much higher contribution than the homogeneous Fenton reaction in the two novel catalysts systems than in the Fh system. On the other hand, the concentrations of Fe^{3+} for all samples increase at the beginning and then start to decrease after 30 min. Previous studies showed that during the degradation of organic contaminants, some acidic intermediates might form and react with Fe^{3+} to form complexes, leading to iron leaching from the heterogeneous catalysts. Afterward, these complexes could be further mineralized, resulting in the returning of Fe^{3+} back to the surface of catalysts [10,56].

In addition, the effect of pH on the degradation of BPA by Fh and 8%Ag/AgBr/Fh was studied (Fig. 8b), and the K_{app} values were calculated using the pseudo-first-order equation (Fig. S6). Compared to Fh in an acid condition (pH = 3; K_{app} = 0.0101 min^{-1}), 8%Ag/AgBr/Fh exhibits a relatively higher photo-Fenton reactivity even at neutral pH (pH = 6.9; K_{app} = 0.0164 min^{-1}). It indicated that the reduction of dissolved Fe^{3+} contributes much less than the reduction of solid Fe(III) in the 8%Ag/AgBr/Fh system. As such, direct solid phase reduction of
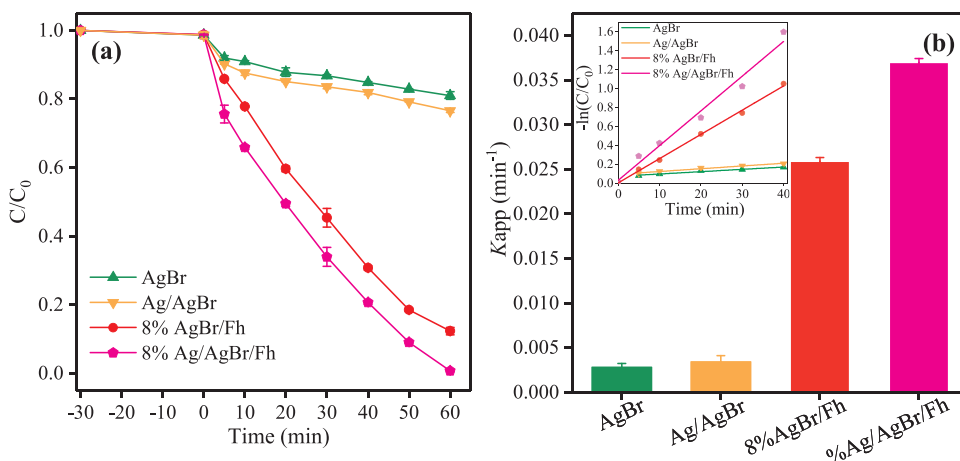

Fig. 7. (a) Degradation kinetics and (b) apparent degradation rate constants of BPA on AgBr and 8%AgBr/Fh before and after reducing Ag nanoparticles under visible light irradiation. Inset of (b): pseudo-first order kinetics for the photocatalytic degradation of BPA on these samples. [Catalyst dosage] = 1 g/L; [BPA] = 30 mg/L; [H_2O_2] = 10 mM; pH = 3.
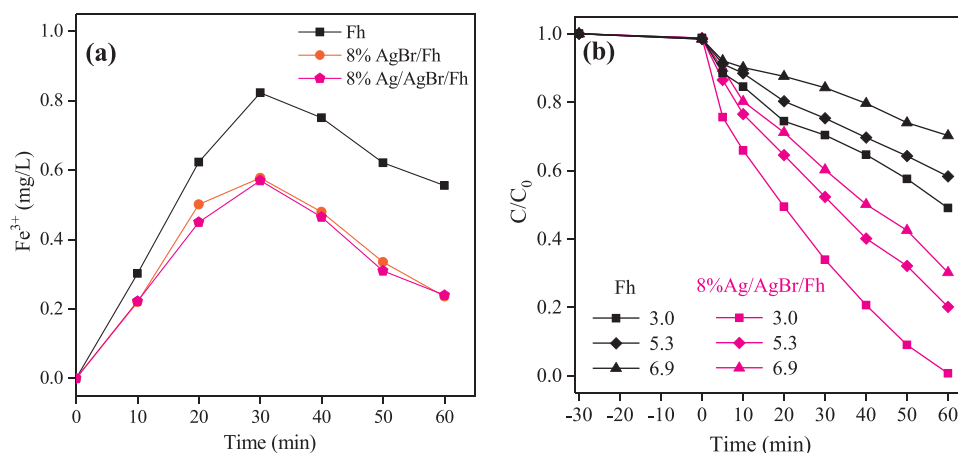
Fig. 8. (a) Dissolved Fe^{3+} concentration in the photo-Fenton catalytic reaction; (b) Effect of pH on degradation of BPA on 8%Ag/AgBr/Fh under visible light irradiation. [Catalyst dosage] = 1 g/L; [BPA] = 30 mg/L; [H_2O_2] = 10 mM.

Fe(III) by injection of photo-generated electrons can enhance the structural stability of the heterogeneous catalysts and reduce the effect of the increased solution pH.

In addition, the effect of catalyst dosage on the degradation of BPA by 8%Ag/AgBr/Fh was also studied (Fig. S7). The degradation of BPA first increases with the increase of dosage from 0.5 to 1 g/L, and then decreases slightly, when the dosage is further increased to 2 g/L. This slight decrease could be due to the high catalyst dosage that would obstruct the penetration of light and bring high turbidity.

Different samples were synthesized by irradiating 8%AgBr/Fh with a mercury lamp at different irradiation time to explore the effect of irradiation time by mercury lamp in the process of sample preparation. The degradation rate of BPA increases evidently as the irradiation time increases from 0 to 0.5 h, but then it increases rather slowly from 0.5 to 3 h (Fig. S8). Therefore, considering the cost, the irradiation time for the deposition of Ag nanoparticles on 8%Ag/AgBr/Fh was set at 0.5 h in this work.

3.3. Decomposition of H_2O_2 and production of ·OH

As shown in Fig. 9, H_2O_2 can hardly be decomposed in the absence of catalysts. The addition of AgBr can accelerate the decomposition of H_2O_2, and Ag/AgBr shows a further increased decomposition rate of H_2O_2, indicating that both AgBr and Ag nanoparticles can generate electrons to decompose H_2O_2 under visible light irradiation. In the

presence of Fh, about 51.2% H_2O_2 can be decomposed within 60 min. The loading of AgBr on the surface of Fh can evidently accelerate the decomposition rate of H_2O_2, with nearly 90.5% H_2O_2 being decomposed by 8%AgBr/Fh. In addition, after depositing Ag nanoparticles, 8%Ag/AgBr/Fh can decompose about 94.6% H_2O_2 within 60 min, which further verifies the positive effect of Ag nanoparticles on the photo-Fenton catalytic reaction. The enhancement of H_2O_2 decomposition rate should be ascribed to the high conversion rate of Fe^{3+}/Fe(III) to Fe^{2+}/Fe(II) due to the photo-generated electrons from AgBr and Ag nanoparticles under the irradiation of visible light, which are discussed in details below.

The concentrations of ·OH in the heterogeneous photo-Fenton reaction were measured using BA as an ·OH probe (Fig. 10). The concentration of ·OH increases obviously after the introduction of AgBr, suggesting that the presence of AgBr could accelerate the generation of ·OH. Noticeably, the ·OH concentration in the 8%AgBr/Fh system reaches 193.8 μmol/L, which is much higher than that in the Fh system (80.6 μmol/L). Furthermore, the ·OH concentration in the 8%Ag/AgBr/Fh system reaches to 210.8 μmol/L. The concentrations of produced ·OH in these three systems are in good agreement with their performance in degradating BPA.

3.4. Effect of initial H_2O_2 concentration on the catalytic efficiency of Fh and 8%Ag/AgBr/Fh

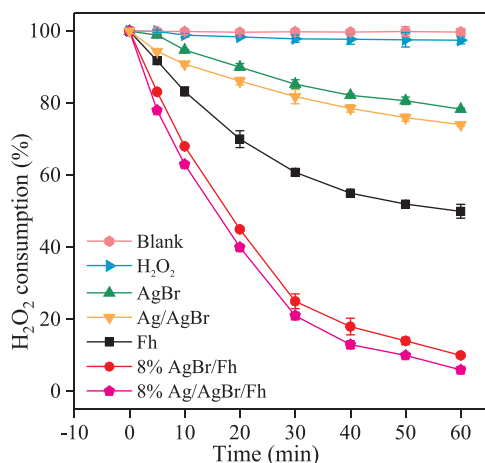In a photo-Fenton reaction, the initial H_2O_2 concentration is a key

Fig. 9. H_2O_2 consumption in the photo-Fenton catalysis over the as-prepared samples. [Catalyst dosage] = 1 g/L; [BPA] = 30 mg/L; [H_2O_2] = 10 mM; pH = 3.
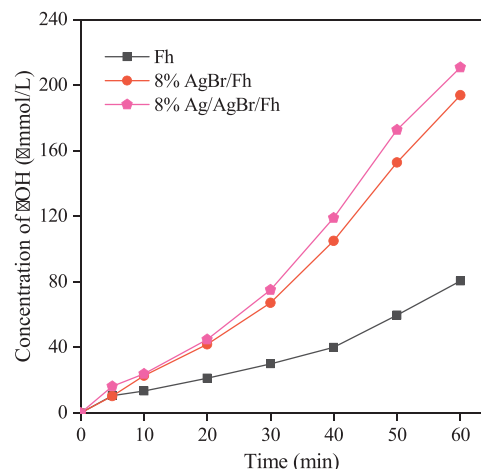

Fig. 10. The concentration of ·OH in the heterogeneous photo-Fenton reaction. [Catalyst dosage] = 1 g/L; [BA] = 10 mM; [H_2O_2] = 10 mM; pH = 3.
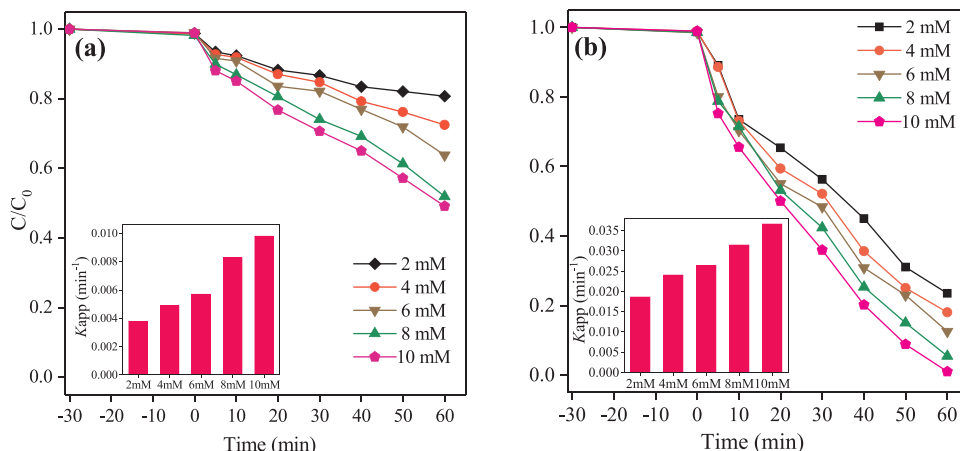
Fig. 11. Effect of H_2O_2 concentration on the degradation of BPA over (a) Fh and (b) 8%Ag/AgBr/Fh. [Catalyst dosage] = 1 g/L; [BPA] = 30 mg/L; pH = 3.
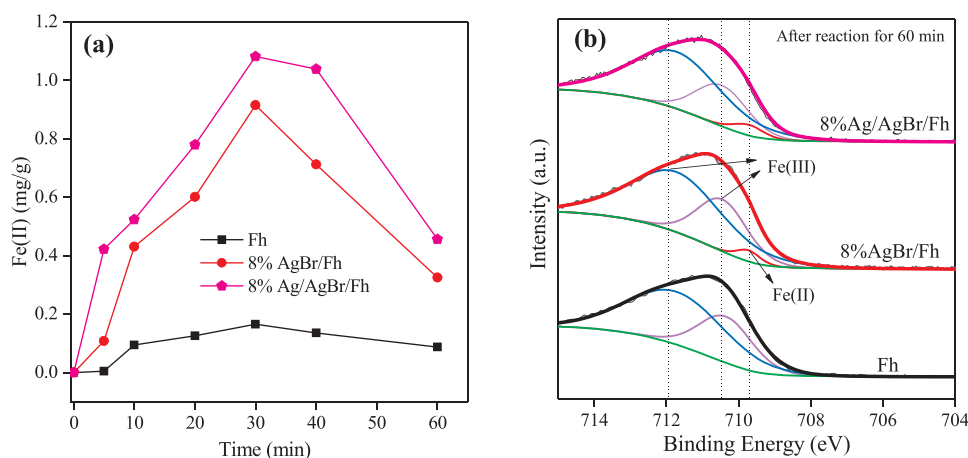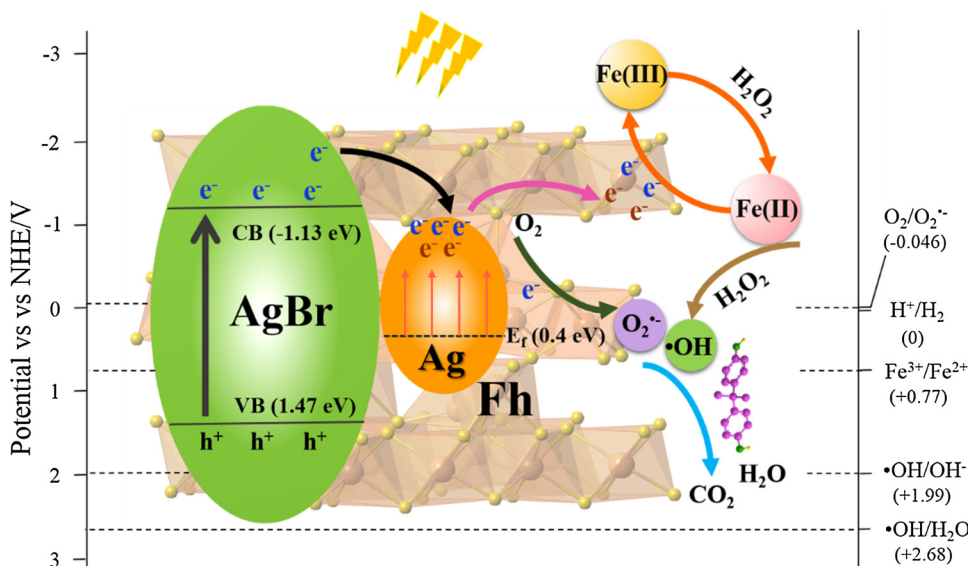

Fig. 12. (a) Concentration of Fe(II) on 8%Ag/AgBr/Fh during the photo-Fenton reaction. [Catalyst dosage] = 1 g/L; [BPA] = 30 mg/L; [H_2O_2] = 10 mM; pH = 3; (b) Fe $2p_{3/2}$ XPS spectra of Fh, 8%AgBr/Fh, and 8%Ag/AgBr/Fh after degradation of BPA for 60 min.

Scheme 1. Possible photo-Fenton catalytic mechanism.

factor that can significantly influence the efficiency of catalysts [57]. As shown in Fig. 11b, with initial H_2O_2 concentration increasing from 2 to 10 mM, the degradation rates of BPA by 8%Ag/AgBr/Fh increase and then begin to decrease after further increasing the H_2O_2 concentration to 12 and 14 mM (Fig. S9), which may be due to that redundant H_2O_2 may consume ·OH. Therefore, the optimal H_2O_2 concentration is 10 mM. Moreover, several degradation experiments with different initial H_2O_2 concentration on Fh were also conducted (Fig. 11a). The

degradation kinetics of BPA by Fh and 8%Ag/AgBr/Fh with different H_2O_2 concentration were fitted with the pseudo-first-order equation. To better compare the effect of H_2O_2 concentration on the photo-Fenton catalytic efficiency of Fh and 8%Ag/AgBr/Fh, the reduction degree of K_{app} in the reaction of different H_2O_2 concentrations (2, 4, 6, and 8 mM) was compared to that of 10 mM (Table S2). The reduction degree of K_{app} in the Fh system is evidently higher than that in the 8%Ag/AgBr/Fh system, with maximum K_{app} reduction degree being 61.2% and 48.6%, respectively, which indicates that the introduction of Ag/AgBr can improve the efficiency of H_2O_2 utilization. Moreover, 8%Ag/AgBr/Fh exhibits much higher photo-Fenton catalytic activity with initial H_2O_2 concentrations of 2 mM ($K_{app} = 0.019 \min^{-1}$) than that of Fh with initial H_2O_2 concentrations of 10 mM ($K_{app} = 0.0098 \min^{-1}$).

As we proposed, Fe(III) can be quickly reduced to Fe(II) by photo-generated electrons from Ag/AgBr, avoiding the consumption of H_2O_2 by Fe^{3+}/Fe(III) (Eqs. (1) and (3)), which should be the reason for the more efficient utilization of H_2O_2 in the 8%Ag/AgBr/Fh system.

3.5. Generation of Fe(II)

As indicated above, we propose the photo-generated electrons from AgBr and Ag nanoparticles under visible light can be transferred to Fh to accelerate the reduction of Fe(III) to Fe(II). Measuring the concentrations of Fe(II) on catalysts during the photo-Fenton reaction can provide direct evidence for our hypothesis, and this experiment has been conducted by totally dissolving catalysts to measure the concentration of Fe^{2+} in aqueous solution. The concentration of Fe(II) on 8%AgBr/Fh is much higher than that on Fh in the whole reaction process (Fig. 12a), indicating that the loading of AgBr can accelerate the reduction of Fe(III) to Fe(II) by the photo-generated electrons from AgBr under visible light. Similar results can be observed in other semiconductor-based heterogeneous photo-Fenton reaction, such as $BiVO_4$/Fh [9]. Moreover, the combining of semiconductors with plasmonic photocatalysts (i.e., 8%Ag/AgBr/Fh) can further enhance the generation of Fe(II), which should be attributed to the abundant photo-generated electrons from both Ag nanoparticles and AgBr; indeed, the strong electron trapping ability of Ag nanoparticles can help in separating the photo-generated electron-hole pairs of AgBr [29,30]. Interestingly, the concentrations of Fe(II) increase evidently in the first 30 min and then decrease for all of the examined samples. At the late stage of the reaction, BPA was degraded and mineralized gradually, resulting in the presence of excess ·OH. The Fe(II) on catalysts may be consumed by the excess ·OH to produce Fe(III) [2,58,59].

To further verify the existence of Fe(II) on these composites, the Fe 2p3/2 XPS spectra of Fh, 8%AgBr/Fh, and 8%Ag/AgBr/Fh after degradation of BPA for 60 min were compared (Fig. 12b). No signals of Fe(II) can be observed in the XPS spectrum of Fh, which may be due to the very low Fe(II) on Fh (Fig. 12a); however, a signal of Fe(II) at 709.64 eV [10,46] appears in both 8%AgBr/Fh and 8%Ag/AgBr/Fh. The Fe 2p XPS spectra of used Fh, 8%AgBr/Fh, and 8%Ag/AgBr/Fh were normalized and then subtracted from used 8% AgBr/Fh to used Fh and from used 8% Ag/AgBr/Fh to used Fh. Both Figs. S3b and S3c show an obvious peak at 709.64 eV, which demonstrates that after introducing Ag/AgBr, the contents of Fe(II) in the 8%AgBr/Fh and 8%Ag/AgBr/Fh system increase compared to that of the pure Fh system. The XPS results further confirm that the photo-generated electrons of Ag/AgBr can accelerate the reduction of Fe(III) to Fe(II) in the photo-Fenton reaction.

3.6. Photo-Fenton catalytic mechanism

On the basis of the experimental results above, Ag/AgBr/Fh shows the highest photo-Fenton catalytic activity for the degradation of BPA, and the possible mechanisms were schematically illustrated (Scheme 1). Under visible light irradiation, AgBr can be stimulated due to its narrow band gap of 2.6 eV [22–25]. As the valence band (VB) of AgBr (1.47 eV) is lower than the redox potential of ·OH/ OH^- (1.99 V vs.

NHE) and ·OH/H_2O (2.68 V vs. NHE) [60], the left holes on the VB of AgBr cannot oxidize OH^- or H_2O to produce ·OH. The conduction band (CB) of AgBr is -1.13 eV (Fig. 6b), which is more negative than the O_2/O_2·- potential (-0.046 V vs. NHE), resulting in the transfer of the photo-generated electrons from AgBr to react with O_2 to form O_2·$^-$. After depositing Ag nanoparticles on the surface of AgBr, Ag nanoparticles can absorb visible light and generate electron-hole pairs due to the SPR effect (Fig. 5a). On the other hand, the CB of AgBr is lower than the Fermi energy of Ag° (0.4 eV) [61,62]. Thus, the photo-generated electrons can be transferred from the CB of AgBr to the surface of Ag nanoparticles, inhibiting the recombination of electron-hole pairs. The potentials of the electrons from both AgBr and Ag nanoparticles are lower than the redox potential of aqueous Fe^{3+}/Fe^{2+} (E° (Fe^{3+}/Fe^{2+}) = +0.77 V vs. NHE) [9], resulting in the reduction of Fe^{3+} by these electrons. As discussed above, the direct heterogeneous Fenton reaction contributes more in the Ag/AgBr/Fh system. Although the specific redox potential of solid Fe(III)/Fe(II) is uncertain, we are confident that the solid Fe(III) can be reduced by the electrons due to the determination of the increased Fe(II) after introducing Ag/AgBr (Fig. 12). In addition, the reduction of Fe^{3+}/Fe(III) by the photo-generated electrons can also reduce the decomposition of H_2O_2 for the generation of Fe^{2+}/Fe(II) (Eqs. (1) and (3)) (Fig. 11) and promote the formation of ·OH (Fig. 10), finally resulting in an obvious improvement of BPA degradation. Meanwhile, the produced O_2·$^-$ may also participate in the degradation and mineralization of BPA.

4. Conclusion

Novel heterogeneous photo-Fenton catalysts (Ag/AgBr/Fh) were synthesized via precipitation and photo reduction methods. The photo-Fenton catalytic activities of AgBr/Fh and Ag/AgBr/Fh composites for the degradation towards BPA are enhanced evidently compared with pure Fh, which should be ascribed to the continuous stream of photo-generated electrons from both AgBr and Ag nanoparticles. On one hand, these electrons can not only accelerate the generation of Fe^{2+}/Fe(II) but also reduce the consumption of H_2O_2, resulting in a significant improvement of catalytic degradation efficiency of BPA by Ag/AgBr/Fh. On the other hand, direct solid phase reduction of Fe(III) by these electrons can enhance the structural stability of the catalysts and broaden the optimal pH range. In addition, the Ag/AgBr/Fh system exhibits higher catalytic activity with lower Fe^{3+} dissolution compared with Fh system, indicating the direct heterogeneous Fenton reaction contributes more in the Ag/AgBr/Fh system. This study may motivate new developments in plasmonic photo-Fenton catalyst methodology and provide a promising strategy for the application of heterogeneous photo-Fenton reaction.

Appendix A. Supplementary data

Supplementary material related to this article can be found, in the online version, at doi:https://doi.org/10.1016/j.apcatb.2018.08.025.

References

[1] A.N. Soon, B.H. Hameed, Desalination 269 (2011) 1–16.
[2] J. He, X. Yang, B. Men, D. Wang, J. Environ. Sci. (China) 39 (2016) 97–109.
[3] X. Hu, B. Liu, Y. Deng, H. Chen, S. Luo, C. Sun, P. Yang, S. Yang, Appl. Catal. B: Environ. 107 (2011) 274–283.
[4] J. Ma, Q. Yang, Y. Wen, W. Liu, Appl. Catal. B: Environ. 201 (2017) 232–240.
[5] O.A. Makhotkina, S.V. Preis, E.V. Parkhomchuk, Appl. Catal. B: Environ. 84 (2008)

821–826.

[6] R.C. Costa, M.F. Lelis, L.C. Oliveira, J.D. Fabris, J.D. Ardisson, R.R. Rios, C.N. Silva, R.M. Lago, J. Hazard. Mater. 129 (2006) 171–178.

[7] T. Xu, R. Zhu, J. Zhu, X. Liang, Y. Liu, Y. Xu, H. He, Catal. Sci. Technol. 6 (2016) 4116–4123.

[8] S. Guo, G. Zhang, J.C. Yu, J. Colloid Interface Sci. 448 (2015) 460–466.

[9] T. Xu, R. Zhu, G. Zhu, J. Zhu, X. Liang, Y. Zhu, H. He, Appl. Catal. B: Environ. 212 (2017) 050–058.

[10] Y. Zhu, R. Zhu, Y. Xi, T. Xu, L. Yan, J. Zhu, G. Zhu, H. He, Chem. Eng. J. 346 (2018) 567–577.

[11] X. Wang, C. Liu, X. Li, F. Li, S. Zhou, J. Hazard. Mater. 153 (2008) 426–433.

[12] X. Zhang, Y. Chen, N. Zhao, H. Liu, Y. Wei, RSC Adv. 4 (2014) 21575–21583.

[13] L. Yu, J. Chen, Z. Liang, W. Xu, L. Chen, D. Ye, Sep. Purif. Technol. 171 (2016) 80–87.

[14] J. Ma, M. Yang, F. Yu, J. Chen, J. Colloid Interface Sci. 444 (2015) 24–32.

[15] T. Xu, R. Zhu, J. Liu, Q. Zhou, J. Zhu, X. Liang, Y. Xi, H. He, J. Mol. Catal. A Chem. 424 (2016) 393–401.

[16] R. Matta, K. Hanna, S. Chiron, Sci. Total Environ. 385 (2007) 242–251.

[17] K. Toda, T. Tanaka, Y. Tsuda, M. Ban, E.P. Koveke, M. Koinuma, S. Ohira, J. Hazard. Mater. 278 (2014) 426–432.

[18] M. Xing, W. Xu, C. Dong, Y. Bai, J. Zeng, Y. Zhou, J. Zhang, Y. Yin, Chemistry 4 (2018) 1359–1372.

[19] T. Xu, R. Zhu, J. Zhu, X. Liang, Y. Liu, Y. Xu, H. He, Appl. Clay Sci. 129 (2016) 27–34.

[20] M.E. Hassan, Y. Chen, G. Liu, D. Zhu, J. Cai, J. Water Process Eng. 12 (2016) 52–57.

[21] S. Ren, C. Chen, Y. Zhou, Q. Dong, H. Ding, Res. Chem. Intermed. 43 (2016) 3307–3323.

[22] H. Xu, Y. Xu, H. Li, J. Xia, J. Xiong, S. Yin, C. Huang, H. Wan, Dalton Trans. 41 (2012) 3387–3394.

[23] M. Abou Asi, C. He, M. Su, D. Xia, L. Lin, H. Deng, Y. Xiong, R. Qiu, X.-z. Li, Catal. Today 175 (2011) 256–263.

[24] H. Zhao, L. Zhang, X. Gu, S. Li, B. Li, H. Wang, J. Yang, J. Liu, RSC Adv. 5 (2015) 10951–10959.

[25] D. Wang, L. Guo, Y. Zhen, L. Yue, G. Xue, F. Fu, J. Mater. Chem. A Mater. Energy Sustain. 2 (2014) 11716–11727.

[26] H. Cheng, B. Huang, P. Wang, Z. Wang, Z. Lou, J. Wang, X. Qin, X. Zhang, Y. Dai, Chem. Commun. (Camb.) 47 (2011) 7054–7056.

[27] Y. Sang, L. Kuai, C. Chen, Z. Fang, B. Geng, ACS Appl. Mater. Interfaces 6 (2014) 5061–5068.

[28] Y. Guan, S. Wang, X. Wang, C. Sun, Y. Huang, C. Liu, H. Zhao, Appl. Catal. B: Environ. 209 (2017) 329–338.

[29] C. Tang, H. Bai, L. Liu, X. Zan, P. Gao, D.D. Sun, W. Yan, Appl. Catal. B: Environ. 196 (2016) 57–67.

[30] X. Yan, X. Wang, W. Gu, M. Wu, Y. Yan, B. Hu, G. Che, D. Han, J. Yang, W. Fan, W. Shi, Appl. Catal. B: Environ. 164 (2015) 297–304.

[31] K. Dai, D. Li, L. Lu, Q. Liu, C. Liang, J. Lv, G. Zhu, Appl. Surf. Sci. 314 (2014) 864–871.

[32] J. Liu, G. Zhang, Phys. Chem. Chem. Phys. 16 (2014) 8178–8192.

[33] J.C. Barreiro, M.D. Capelato, L. Martin-Neto, H.C. Bruun Hansen, Water Res. 41 (2007) 55–62.

[34] P.V. Nidheesh, RSC Adv. 5 (2015) 40552–40577.

[35] Z. Yan, Z. Xu, J. Yu, M. Jaroniec, Environ. Sci. Technol. 49 (2015) 6637–6644.

[36] V.F. Samanidou, M.A. Frysali, I.N. Papadoyannis, J. Liq. Chromatogr. Relat. Technol. 37 (2014) 247–258.

[37] R.M. Sellers, Analyst 105 (1980) 950–954.

[38] Q. Zhou, Y. Li, L. Wang, B. Liao, Fiber Glass (2016).

[39] S.H. Joo, A.J. Feitz, D.L. Sedlak, T.D. Waite, Environ. Sci. Technol. 39 (2005) 1263–1268.

[40] C.R. Keenan, D.L. Sedlak, Environ. Sci. Technol. 42 (2008) 1262–1267.

[41] Q. Zhu, W.-S. Wang, L. Lin, G.-Q. Gao, H.-L. Guo, H. Du, A.-W. Xu, J. Phys. Chem. C 117 (2013) 5894–5900.

[42] S. Huang, Y. Xu, M. Xie, Q. Liu, H. Xu, Y. Zhao, M. He, H. Li, RSC Adv. 7 (2017) 30845–30854.

[43] Y. Xu, H. Xu, J. Yan, H. Li, L. Huang, Q. Zhang, C. Huang, H. Wan, PCCP 15 (2013) 5821–5830.

[44] X. Li, D. Tang, F. Tang, Y. Zhu, C. He, M. Liu, C. Lin, Y. Liu, Mater. Res. Bull. 56 (2014) 125–133.

[45] Z. Zhao, M. Wang, T. Yang, M. Fang, L. Zhang, H. Zhu, C. Tang, Z. Huang, J. Mol. Catal. A Chem. 424 (2016) 8–16.

[46] Y. Lee, W. Lee, J. Hazard. Mater. 178 (2010) 187–193.

[47] R.K. Vempati, R.H. Loeppert, D.L. Cocke, Solid State Ion. 26 (1990) 179-179.

[48] J. Cao, Y. Zhao, H. Lin, B. Xu, S. Chen, Mater. Res. Bull. 48 (2013) 3873–3880.

[49] C. Tang, J. Zhu, Q. Zhou, J. Wei, R. Zhu, H. He, J. Phys. Chem. C 118 (2014) 26249–26257.

[50] C. Zeng, M. Guo, B. Tian, J. Zhang, Chem. Phys. Lett. 575 (2013) 81–85.

[51] P. Zhang, P. Wu, S. Bao, Z. Wang, B. Tian, J. Zhang, Chem. Eng. J. 306 (2016) 1151–1161.

[52] T. Li, Y. He, H. Lin, J. Cai, L. Dong, X. Wang, M. Luo, L. Zhao, X. Yi, W. Weng, Appl. Catal. B: Environ. 138-139 (2013) 95–103.

[53] H. Zeng, X. Liu, T. Wei, X. Li, T. Liu, X. Min, Q. Zhu, X. Zhao, J. Li, RSC Adv. 7 (2017) 23787–23792.

[54] Q. Sun, Y. Hong, Q. Liu, L. Dong, Appl. Surf. Sci. (2017).

[55] Y. Liu, W. Jin, Y. Zhao, G. Zhang, W. Zhang, Appl. Catal. B: Environ. 206 (2017) 642–652.

[56] J. Chen, L. Zhu, Sep, Purif. Technol. 67 (2009) 282–288.

[57] J. Herney-Ramirez, M.A. Vicente, L.M. Madeira, Appl. Catal. B: Environ. 98 (2010) 10–26.

[58] C.K. Duesterberg, T.D. Waite, Environ. Sci. Technol. 41 (2007) 4103–4110.

[59] Christopher K. Duesterberg, William J. Cooper, T. David Waite, Environ. Sci. Technol. 39 (2005) 5052.

[60] S. Patnaik, D.P. Sahoo, K. Parida, Renew. Sustain. Energy Rev. 82 (2018) 1297–1312.

[61] F. Dong, Q. Li, Y. Zhou, Y. Sun, H. Zhang, Z. Wu, Dalton Trans. 43 (2014) 9468–9480.

[62] D.P. Sahoo, S. Patnaik, D. Rath, K.M. Parida, Inorg. Chem. Front. 5 (2018) 879–896.